**TITLE:** # LFI OPTICAL INTERFACES

**DOC. TYPE:** TECHNICAL NOTE

**PROJECT REF.:** PL-LFI-PST-TN-034 **PAGE:** I of VI, 20

**ISSUE/REV.:** 1.0 **DATE:** June 2002

| | | | |
|---|---|---|---|
| Prepared by | A. MENNELLA, F.VILLA, M. SANDRI, C. BURIGANA<br>LFI<br>Project System Team<br><br>M. BERSANELLI<br>LFI<br>Instrument Scientist | Date:<br><br>Signature: | June 28th, 2002 |
| Agreed by | C. BUTLER<br>LFI<br>Program Manager | Date:<br><br>Signature: | June 28th, 2002 |
| Approved by | N. MANDOLESI<br>LFI<br>Principal Investigator | Date:<br><br>Signature: | June 28th, 2002 |

# DISTRIBUTION LIST

| Recipient | Company / Institute | E-mail address | Sent |
|---|---|---|---|
| ALIPPI, E. | LABEN – Vimodrone | ealippi@webmail.laben.it | Yes |
| BANDAY, A. | MPA, Garching | banday@mpa-garching.mpg.de | Yes |
| BARTELMANN, M. | MPA, Garching | msb@mpa-garching.mpg.de | Yes |
| BERSANELLI, M. | UNIMI – Milano | marco@ifctr.mi.cnr.it | Yes |
| BURIGANA, C. | IASF-CNR Bologna | burigana@tesre.bo.cnr.it | Yes |
| BUTLER, R.C. | IASF – Sezione di Bologna | butler@tesre.bo.cnr.it | Yes |
| CHARRA, J. | IAS - Paris | jacques.charra@ias.u-psud.fr | Yes |
| COLLAUDIN, B. | ALCATEL | Bernard.Collaudin@space.alcatel.fr | Yes |
| CRONE, J. | ESA – Noordwijk | Gerald.Crone@esa.int | Yes |
| DE CHAMBURE, D. | ESA - Noordwijk | Daniel.de.Chambure@esa.int | Yes |
| DE MAAGT, P. | ESA – Noordwijk | Peter.de.Maagt@esa.int | Yes |
| DE ZOTTI, G. | OAP, Padova | dezotti@pd.astro.it | Yes |
| DUBRUEL, D. | ALCATEL | denis.dubruel@space.alcatel.fr | Yes |
| GAIER, T. | JPL, Pasadena | gaier@merlin.jpl.nasa.gov | Yes |
| GORSKI, K. | ESO, Garching | kgorski@eso.org | Yes |
| HOYLAND, R. | IAC, Tenerife | rjh@ll.iac.es | Yes |
| LAWRENCE, C. | JPL, Pasadena | lawrence.a.wade@jpl.nasa.gov | Yes |
| MAINO, D. | SISSA, Trieste | maino@ts.astro.it | Yes |
| MANDOLESI, N. | IASF – Sezione di Bologna | reno@tesre.bo.cnr.it | Yes |
| MARTI-CANALES, J. | ESA – Noordwijk | Javier.Marti.Canales@esa.int | Yes |
| MENNELLA, A. | IASF – Sezione di Milano | Mennella@mi.iasf.cnr.it | Yes |
| NOORGAARD NIELSEN, H.U. | DSRI | hunn@dsri.dk | Yes |
| PASIAN, F | OAT – Trieste | pasian@ts.astro.it | Yes |
| PASSVOGEL, T. | ESA – Noordwijk | Thomas.Passvogel@esa.int | Yes |
| POLEGRE, A.M. | ESA – Noordwijk | Arturo.Martin.Polegre@esa.int | Yes |
| RITI, J-B | ALCATEL | Jean-Bernard.Riti@space.alcatel.fr | Yes |
| SANDRI, M. | IASF – Sezione di Bologna | sandri@tesre.bo.cnr.it | Yes |
| SEIFFERT, M. | JPL, Pasadena | michael.d.seiffert@jpl.nasa.gov | Yes |
| TAUBER, J. | ESA – Noordwijk | jtauber@rssd.esa.int | Yes |
| TOFANI, G. | IRA – Bologna | tofani@arcetri.astro.it | Yes |
| TUOVINEN, J. | Millilab, Finland | jussi.tuovinen@vtt.fi | Yes |
| VALENZIANO, L. | IASF – Sezione di Bologna | valenzia@tesre.bo.cnr.it | Yes |
| VILLA, F. | IASF – Sezione di Bologna | villa@tesre.bo.cnr.it | Yes |
| VITTORIO, N. | Univ. “Tor Vergata”, Roma | vittorio@roma2.infn.it | Yes |
| WILKINSON, A. | JBO, UK | aw@jb.man.ac.uk | Yes |
| LFI System PCC | IASF – Sezione di Bologna | lfispcc@tesre.bo.cnr.it | Yes |

# CHANGE RECORD

| Issue | Date | Sheet | Description of Change | Release |
|---|---|---|---|---|
| 1.0 | June 2002 | All | First Issue of the Document | === |
| | | | | |
| | | | | |
| | | | | |
| | | | | |
| | | | | |
| | | | | |
| | | | | |
| | | | | |
| | | | | |
| | | | | |
| | | | | |
| | | | | |
| | | | | |
| | | | | |
| | | | | |
| | | | | |
| | | | | |
| | | | | |
| | | | | |
| | | | | |
| | | | | |
| | | | | |
| | | | | |
| | | | | |
| | | | | |
| | | | | |
| | | | | |
| | | | | |
| | | | | |
| | | | | |
| | | | | |
| | | | | |

# TABLE OF CONTENTS

# LIST OF TABLES

# LIST OF FIGURES

# 1 INTRODUCTION AND SCOPE

The Low Frequency Instrument is coupled to the Planck Telescope by 23 Corrugated Feed Horns. The coupling between the feeds and the external environment constitutes the LFI Optical Interfaces. In the ideal case, the external environment is composed by the Planck Telescope only. In the real case, because of the imperfect feed response and coupling between the feed and Telescope, the environment is constituted of all the satellite surfaces (including the telescope) and celestial objects which can emit, reflect, or scatter, radiation within the operational bandwidth of the LFI detectors.

The optical interfaces have a potentially strong effect on the LFI scientific capabilities because are related to the angular resolution and to the level of some systematic effects, *"Straylight",* in this case.

The requirements of the optical interfaces have an impact on the Feed horn design, as well as on the thermal stability of the spacecraft. In the ideal case the optical interfaces have an impact on the angular resolution only. Ideal feeds, and telescope are assumed. This means no self – emission of surfaces and no diffraction effects on optical elements. In the real case, the optical interfaces have an impact also on the shape of the main beam (ellipticity), on the non perfect off–axis optical response on the sky (External straylight), and on the imperfect off – axis rejection of the feeds which detect the emission of the surrounding surfaces (Internal Straylight). The guideline for designing the optical interface is the following:

> The Optical Interfaces must be designed in order to obtain the best angular resolution achievable compatible with straylight (both internal and external) requirements.

In fact, since the PLANCK telescope design is fixed, the angular resolution depends on the illumination by the feeds of the edges of both the primary and sub-reflector (Edge Taper). An improvement of the angular resolution implies a degradation of the straylight rejection.

| | Main Beam Response | | Stray Light | |
|---|---|---|---|---|
| | Angular Resolution | Ellipticity | External | Internal |
| **Ideal Case** | ✓ | × | × | × |
| **Real Case** | ✓ | ✓ | ✓ | ✓ |

***Table 1-1*** *– Impact of the Optical Interfaces: Ideal and Real Case.*

The aim of this technical note is to translate the scientific requirements of LFI, when applicable, into requirements on the Optical Interfaces and specifically into requirements on the instrument and satellite designs and thermal stabilities.

# 2 APPLICABLE DOCUMENTS

[AD 1] M.Bersanelli, M.Seiffert, R.Hoyland, A.Mennella, *"Planck – LFI scientific Requirements"*, PL-LFI-PST-SP-011, Issue 2.0 (2002)

[AD 2] FIRST – Planck Project System Team, *"PLANCK Telescope Design Specification"*, SCI–PT–RS–07024, Issue 1.0, (2000)

[AD 3] Herschel/Planck Project System Team, *Herschel/Planck Instrument Interface Document – IID PART A*, Doc. No.: SCI-PT-IIDA-04624, Issue/Rev. No. : 2/0, 31/07/2001

# 3 REFERENCE DOCUMENTS

[RD 1] N.Mandolesi, M.Bersanelli, C.Burigana, K.M.Górski, E.Hivon, D.Maino, L.Valenziano, F.Villa, M.White, *"On the performance of Planck-like telescopes versus mirror aperture*", Astron. Astrophys. Suppl. Ser. **145**, 323-340 (1998)

[RD 2] C. Burigana, D. Maino, N. Mandolesi, E. Pierpaoli, M. Bersanelli, L. Danese, M.R. Attolini, "*Beam distortion effects on anisotropy measurements of the cosmic microwave background"*, Astron. Astrophys. Suppl. Ser. **130**, 551-560 (2000)

[RD 3] C.Burigana, D.Maino, K.M.Górski, N.Mandolesi, M.Bersanelli, F.Villa, L.Valenziano, B.D.Wandelt, M.Maltoni and E.Hivon, *"PLANCK LFI: Comparison between Galaxy Straylight Contamination and other systematic effects"*, A&A **373**, 345-358 (2001)

[RD 4] P. de Maagt, A. Martin Polegre & G. Crone, "*PLANCK: Straylight Evaluation of the Carrier Configuration",* ESA Technical Note, PT–TN–05967, Issue 2 (2000)

[RD 5] C.Burigana, D.Maino, N.Mandolesi, F.Villa, L.Valenziano, M.Bersanelli, L.Danese, L.Toffolatti, & F.Argueso, *"On Planck simulations: towards "2-nd order" analyses",* Astrophysical Letters and Comm., **37**, 253-258, (2000)

[RD 6] ASPI Hershel / Planck Team, "*Planck PLM Design Report"*, HP-3-ASPI-RP-0050, Issue 1.0, (2001)

[RD 7] C.Burigana, P.Natoli, N.Vittorio, N.Mandolesi, M.Bersanelli, *"Straylight Contamination from Internal Solar System Bodies in PLANCK-LFI Observations*", Int. Rep. ITeSRE 272/2000 (2000)

[RD 8] C.Burigana, P.Natoli, N.Vittorio, N.Mandolesi, M.Bersanelli, *"In-flight main beam reconstruction for PLANCK-LFI*", Experimental Astronomy, in press, astro-ph/0012273. (2000)

[RD 9] M. Sandri, F. Villa, *"Planck/LFI: Main Beam Locations and Polarization Alignment for the LFI Baseline FPU"*, PL-LFI-PST-TN-027 (2001), Issue/Rev 1.0

[RD 10] C. Burigana, M. Malaspina, N. Mandolesi, L. Danese, D. Maino, M. Bersanelli, M. Maltoni, *A Preliminary Study on Destriping Techniques of PLANCK LFI Measurements Versus Observational Strategy*, Int. Rep. ITeSRE 198/1997, astro-ph/9906360 (1997)

[RD 11] Maino, D., Burigana, C., Gorski, K.M., Mandolesi, N., Bersanelli, M., *Removing 1/f noise stripes in cosmic microwave background anisotropy observations,* Astronomy and Astrophysics, **387**, pp. 356–365 (2002)

# 4 ANGULAR RESOLUTION

The angular resolution has a direct, strong impact on the main scientific objective of LFI [AD 1]. It is limited by the Planck telescope size and overall optical design. Due to the fundamental role of the angular resolution, requirements and goals have been set.

The goal "*effective angular resolution*" at the four LFI frequencies are 10, 14, 24 and 30 arcmin at 100, 70, 44 and 30 GHz, respectively. The corresponding requirement values are 12, 17, 29 and 36 arcmin.

| | 30GHz | 44GHz | 70GHz | 100GHz |
|---|---|---|---|---|
| Goal angular resolution | 30' | 24' | 14' | 10' |
| Required angular resolution | 36' | 29' | 17' | 12' |

***Table 4-1*** *– Angular Resolution: LFI Goal and Requirements*

The ring-like disposition of the LFI feeds and beams is reported in Figure 4-1. In Table 4-2, the main beam characteristics, as derived from optical simulations, are reported. These values have been calculated on the basis of the Edge Taper baseline values[1].

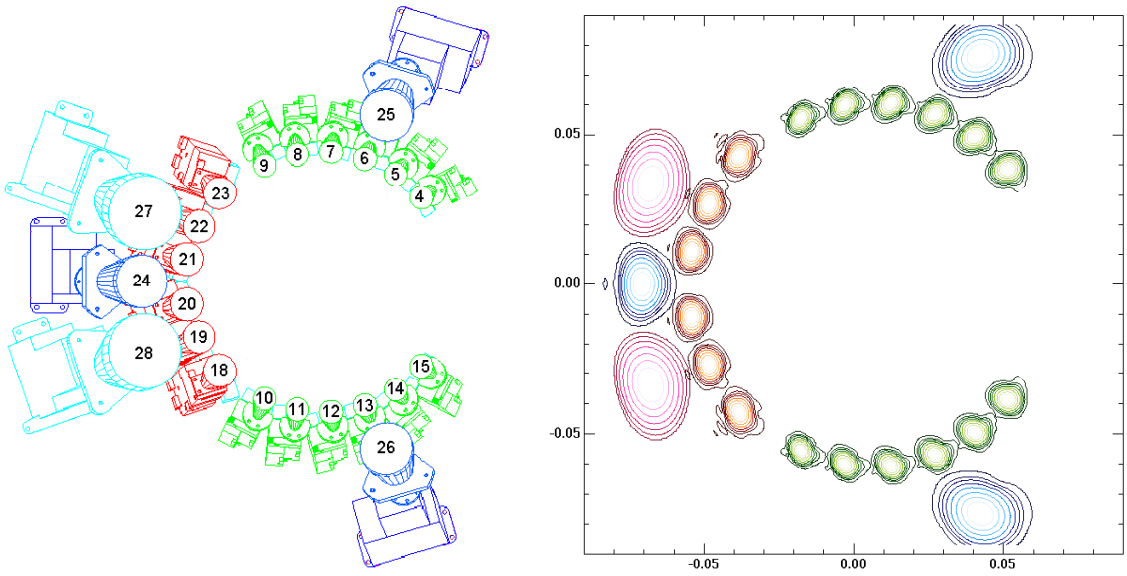


***Figure 4-1*** *– Layout of the LFI Focal Plane Unit (left) and map of the main beams on the sky (right).*

[1] The Edge Taper constraints are based on the ESA 30 GHz full pattern simulation, and are conservative requirements for the feeds at frequencies >30 GHz. An optimisation will be carried out for each individual feed.

| FH # | ET (dB @ ° ) | FWHM (arcmin) | | e | Freq ( GHz ) |
|---|---|---|---|---|---|
| | | min | max | | |
| 4 | 28.1 @ 24 | 11.88 | 13.68 | 1.15 | 100 |
| 5 | 27.4 @ 24 | 11.40 | 13.20 | 1.16 | 100 |
| 6 | 27.7 @ 24 | 11.16 | 13.20 | 1.18 | 100 |
| 7 | 27.6 @ 24 | 10.56 | 12.84 | 1.22 | 100 |
| 8 | 26.8 @ 24 | 10.08 | 12.36 | 1.23 | 100 |
| 9 | 25.5 @ 24 | 9.84 | 11.88 | 1.25 | 100 |
| 10 | 25.5 @ 24 | 9.84 | 11.88 | 1.25 | 100 |
| 11 | 26.8 @ 24 | 10.08 | 12.36 | 1.23 | 100 |
| 12 | 27.6 @ 24 | 10.56 | 12.96 | 1.23 | 100 |
| 13 | 27.7 @ 24 | 11.16 | 13.20 | 1.18 | 100 |
| 14 | 27.4 @ 24 | 11.40 | 13.44 | 1.18 | 100 |
| 15 | 28.1 @ 24 | 11.88 | 13.68 | 1.15 | 100 |
| 18 | 20.5 @ 22 | 12.36 | 15.72 | 1.27 | 70 |
| 19 | 23.1 @ 22 | 12.60 | 16.08 | 1.28 | 70 |
| 20 | 25.0 @ 22 | 12.60 | 16.44 | 1.30 | 70 |
| 21 | 25.0 @ 22 | 12.60 | 16.44 | 1.30 | 70 |
| 22 | 23.1 @ 22 | 12.60 | 16.08 | 1.28 | 70 |
| 23 | 20.5 @ 22 | 12.36 | 15.72 | 1.27 | 70 |
| 24 | 30.0 @ 22 | 20.04 | 27.84 | 1.39 | 44 |
| 25 | 30.0 @ 22 | 25.32 | 31.68 | 1.25 | 44 |
| 26 | 30.0 @ 22 | 25.32 | 31.68 | 1.25 | 44 |
| 27 | 30.0 @ 22 | 29.16 | 40.68 | 1.40 | 30 |
| 28 | 30.0 @ 22 | 29.16 | 40.68 | 1.40 | 30 |

***Table 4-2*** *– LFI Main beam Characteristics based on the Edge Taper baseline values (column ET). The Minimum* (min)*, Maximum of the angular resolution are reported. The ellipticity, e, has been calculated as the ratio* FWHMmax/FWHMmin*. The associated error on the FWHM values is ± 0.06 arcmin.*

## 4.1 DEFINITION OF THE "EFFECTIVE ANGULAR RESOLUTION"

Because of the aberrations, the main beam exhibits a non–gaussian non–symmetric shape. Then the Full Width Half Maximum (FWHM) is not univocally determined. For CMB anisotropy measurements an "effective angular resolution" can be defined as the FWHM of a perfect (symmetric gaussian) beam which

produces the same signal of the distorted beam when the CMB field is observed[2] [RD 1] [RD 2]. The 1st order effect of the aberrations is to degrade the angular resolution of the beam.
Instead of the FWHMeff we can simply evaluate the angular resolution by taking the average FWHM of the distorted beam. The average FWHM has been calculated in three different way, straightforward from the minimum and maximum values reported in Table 4-2:

1. ARITHMETIC AVERAGE: by taking the average value between the maximum and minimum of the FWHM of the distorted beam. $\text{ave}_A = \frac{\text{FWHM}_{\text{MIN}} + \text{FWHM}_{\text{MAX}}}{2}$;
2. QUADRATIC AVERAGE: by taking the quadratic mean between the maximum and minimum of the FWHM of the distorted beam. $\text{ave}_Q = \sqrt{\frac{\text{FWHM}_{\text{MIN}}^2 + \text{FWHM}_{\text{MAX}}^2}{2}}$;
3. EQUAL AREA AVERAGE[3]: the distorted beam exhibits the same beam area of a symmetric beam with a FWHM defined as follows: $\text{ave}_E = \sqrt{\text{FWHM}_{\text{MIN}} \cdot \text{FWHM}_{\text{MAX}}}$.

| FH | FWHM (arcmin) | | | | | FH | FWHM (arcmin) | | | | |
|---|---|---|---|---|---|---|---|---|---|---|---|
| # | min | max | $\text{ave}_A$ | $\text{ave}_Q$ | $\text{ave}_E$ | # | min | max | $\text{ave}_A$ | $\text{ave}_Q$ | $\text{ave}_E$ |
| 4 | 11.88 | 13.68 | 12.78 | 12.81 | 12.75 | 18 | 12.36 | 15.72 | 14.04 | 14.14 | 13.94 |
| 5 | 11.40 | 13.20 | 12.30 | 12.46 | 12.38 | 19 | 12.60 | 16.08 | 14.34 | 14.45 | 14.23 |
| 6 | 11.16 | 13.20 | 12.18 | 12.22 | 12.14 | 20 | 12.60 | 16.44 | 14.52 | 14.65 | 14.39 |
| 7 | 10.56 | 12.84 | 11.70 | 11.76 | 11.64 | 21 | 12.60 | 16.44 | 14.52 | 14.65 | 14.39 |
| 8 | 10.08 | 12.36 | 11.22 | 11.28 | 11.16 | 22 | 12.60 | 16.08 | 14.34 | 14.45 | 14.23 |
| 9 | 9.84 | 11.88 | 10.68 | 10.75 | 10.61 | 23 | 12.36 | 15.72 | 14.04 | 14.14 | 13.94 |
| 10 | 9.84 | 11.88 | 10.68 | 10.75 | 10.61 | 24 | 20.04 | 27.84 | 23.94 | 24.26 | 23.62 |
| 11 | 10.08 | 12.36 | 11.22 | 11.28 | 11.16 | 25 | 25.32 | 31.68 | 28.50 | 28.68 | 28.32 |
| 12 | 10.56 | 12.96 | 11.76 | 11.82 | 11.70 | 26 | 25.32 | 31.68 | 28.50 | 28.68 | 28.32 |
| 13 | 11.16 | 13.20 | 12.18 | 12.22 | 12.14 | 27 | 29.16 | 40.68 | 34.92 | 35.39 | 34.44 |
| 14 | 11.40 | 13.44 | 12.42 | 12.46 | 12.38 | 28 | 29.16 | 40.68 | 34.92 | 35.39 | 34.44 |
| 15 | 11.88 | 13.68 | 12.78 | 12.81 | 12.75 | | | | | | |

***Table 4-3:*** *Calculated average FWHM. The three definitions, arithmetic, quadratic, and equal–area have been applied. The associated error is ± 0.06 arcmin.*

For comparison, the 100 GHz average FWHM ($\text{ave}_A$, $\text{ave}_Q$, and $\text{ave}_E$) have been plotted and reported in Figure 4-2. It is noticed that the arithmetical mean is between the other two, and small differences exist between the $\text{ave}_A$ and the arithmetic mean of $\text{ave}_Q$ and $\text{ave}_E$. In fact, the average can be written in the following way:

$$\frac{\text{ave}_Q + \text{ave}_Q}{2} = \text{ave}_A - \left\{ \frac{1}{2} \text{FWHM}_{\text{min}} \left( 1 + e - \sqrt{e} - \frac{\sqrt{2}}{2} \sqrt{1 + e^2} \right) \right\}$$

[2] In this case "observed" means simulated observation taking into account the scanning strategy and the CMB expected anisotropy map.
[3] The meaning of "equal area" derives from [RD11]. For gaussian elliptical beams FWHMeff = $\text{FWHMave}_E$

or alternatively

$$\frac{\mathrm{ave}_Q + \mathrm{ave}_Q}{2} = \mathrm{ave}_A - \left\{ \frac{1}{2} \mathrm{FWHM}_{max} \left( \frac{1+e}{e} - \sqrt{\frac{1}{e}} - \frac{\sqrt{2}}{2} \sqrt{1 + \frac{1}{e^2}} \right) \right\}$$

The term between parentheses is small $(\approx 10^{-4} \div 10^{-5})$, zero in the case of perfect symmetric beam (ellipticity $e = 1$).
Moreover, it is clear that only some of the beams exhibit an angular resolution compatible with the requirements, and none of them with the goal. For this reason a trade off between the angular resolution and edge taper (i.e. straylight) is in progress.
As show in Table 4-3 and Figure 4-2, the differences between the three "average FWHM" are 2.7% at 30GHz and less than 1.3% at 100 GHz. Although it is important include in the data analysis the detailed information of the beam shape, these small differences are not a concern for the angular resolution requirements. **We use as the reference FWHM the arithmetic average.**

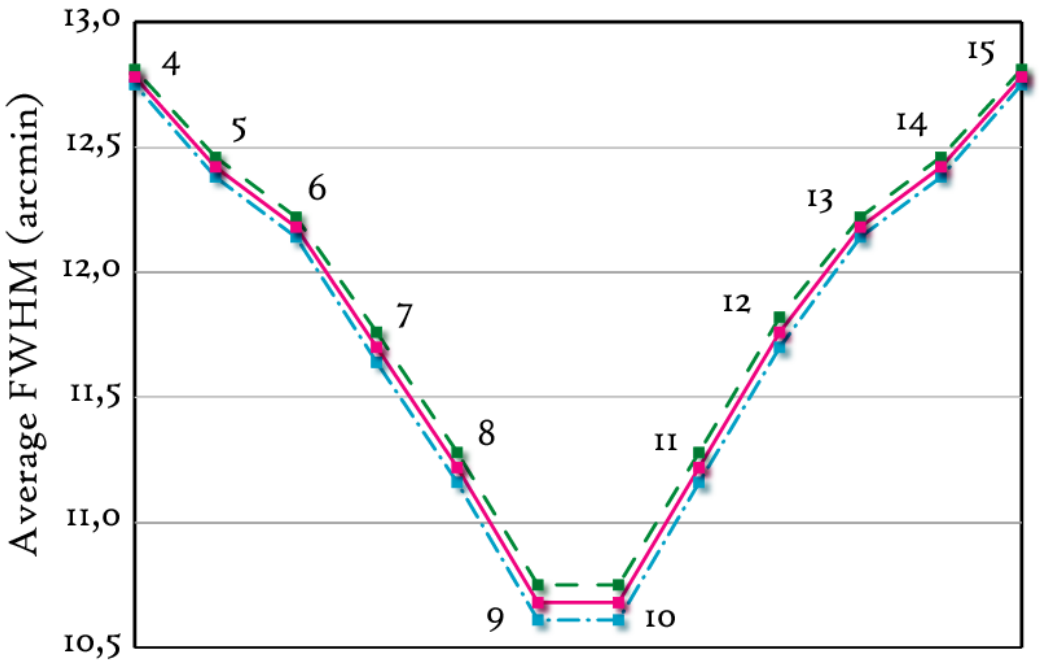


***Figure 4-2:*** *Comparison between different definitions of the average FWHM for the 100 GHz beams. The blue line (dashed – dot) is the equal area average. The red line (solid) is the arithmetic average. The green line (dashed) is the quadratic average. Numbers on data points report the ID of the feeds (i.e. beams).*

# 5 STRAYLIGHT

"Straylight" is defined for the Planck instruments as the radiative power that reaches a detector within its RF bandwidth, and that does not originate from sources in the main beam [AD 3]. Straylight induces a signal that is indistinguishable from signals induced by sources located in the main beam. *Variations* in straylight are a source of systematic error. In the context of PLANCK-LFI we can consider two main types of straylight, according to its origin: *External Straylight*, i.e. stray radiation coming from astrophysical sources, and *Internal Straylight*, i.e. radiation generated by emissive surfaces of the satellite itself.

In [AD 1] we have provided a detailed systematic error budget in which the contributions coming from straylight radiation are detailed. This straylight error budget (in terms of maximum error per pixel in the final maps) is reported in the following table:

| Source | % of $\delta T_{r\text{-}sec}$ | Error from spin synch. signals (μK) | Error from periodic signals (μK) |
|---|---|---|---|
| External Straylight | N/A | 1* | N/A |
| Internal Straylight | 4.5% | 1 | 0.9 |

*In this case we require that any external straylight signal coming from outside data from outside the Galactic plane (±10° around the equator) and from outside a region of TBD deg around the main celestial sources will be less than 1 μK

***Table 5-1*** *– Budget of straylight-induced systematic errors*

To understand and quantify the impact of straylight on PLANCK-LFI we consider two different levels: (i) the evaluation of the effect of straylight fluctuations on the signal measured by the radiometers and (ii) the evaluation of the effect of fluctuations in the measured signal on the final LFI maps (in terms of maximum error per pixel). The first level is clearly dependent on the source of straylight radiation and on the characteristics of the beam patterns, while the second depends only on the period of the effect and on the scan strategy, so that it can be treated independently from the source. Therefore, before analysing in detail the effect of different types of straylight we start with a discussion of the effect of periodic signal fluctuations on the final LFI maps.

## 5.1 FROM A TOD TO THE MAP. THE IMPACT OF RADIOMETER SIGNAL FLUCTUATIONS ON FINAL MAPS

Let us start considering a sinusoidal fluctuation in the radiometer output signal, i.e.: $\delta T(\nu_f, t) = A\cos(2\pi\nu_f t)$, where $\nu_f$ and $A$ represent the fluctuation frequency and amplitude, respectively.

If we now consider that during a scan circle each pixel will be measured $N \approx 60$ times then the damping factor $F$ of the fluctuation after $N$ consecutive spin redundant observations of the same pixel is of the order:

$$F^{-1} = \frac{\sin(\pi\nu_f\tau)}{\pi\nu_f\tau}\frac{1}{N}\sum_{j=1}^{N}\cos\left(2\pi j\nu_f/\nu_{\text{spin}}\right) \qquad \textbf{(2-1)}$$

where $\tau$ is the beam integration time and $\nu_{spin}$ the spin frequency. In general we can consider three different classes of fluctuations, i.e.:

1. *Random* fluctuations. In this case the damping factor is proportional to the square root of the pixel integration time;
2. *fast* (non-random) fluctuations ($\nu_f > 1/\tau$); in this case the term $F^{-1} \approx \sin(\pi\nu_f\tau)/\pi\nu_f\tau \leq 1$, i.e. the fluctuation is completely uncorrelated with the spin and the damping is controlled by the pixel integration time;
3. *slow* (non-random) fluctuations ($\nu_f << 1/\tau$); in this case the term $\sin(\pi\nu_f\tau)/\pi\nu_f\tau \approx 1$ and $F \approx N\left[\sum_{j=1}^{N}\cos\left(2\pi\nu_f/\nu_{spin}\right)\right]^{-1}$. Here we may have correlation between the fluctuation and the spin (including the spin synchronous case), and the damping is controlled by the sampling strategy rather than by the pixel integration time.

If we now consider the case of slow fluctuations (which are more relevant in PLANCK compared to fast non-random fluctuations) then we can identify the following two main cases:

1. $\nu_{spin} / \nu_f \neq k$ ($k$ integer, i.e. non spin-synchronous). In this case if $N$ is sufficiently large, we derive the following simple (approximated) expression for the damping factor after a given time $t$:

$$F \approx N\left|\sin\left(\pi\nu_f/\nu_{spin}\right)\right| \approx \frac{N\pi}{\nu_{spin}}\nu_f \quad \text{for} \quad \pi\nu_f << \nu_{spin} \qquad \textbf{(2-2)}$$

   which shows that for "slow" periodic fluctuations the damping factor increases linearly with the frequency of the oscillation.
2. $k\ \nu_f = \nu_{spin}$ (with $k$ integer, i.e. spin synchronous effect). In this case there is no damping of the fluctuation, and $F = 1$.

Of course the damping factor $F$ at the end of the mission will not be constant throughout the map, but will be distributed in the observed pixels in a non trivial way, which depends on the scanning strategy and feed geometry in the focal plane. A rough analytical estimation of its lower limit, however, can be obtained from equation **(2-2)** with $N = 60 \times \theta_{HPBW} / \theta_{rep}$ where $\theta_{rep}$ is the spacecraft repointing angle (currently 2.5').

In the more general case in which we have a systematic effect of arbitrary shape then we can decompose it in spectral components of amplitude $A_j$ and frequency $\nu_j$ so that the final peak-to-peak effect on the map (without considering the application of removal algorithms) is:

$$\left\langle \delta T^{p-p} \right\rangle \sim 2\left[\frac{1}{N \times \theta_{HPBW}/\theta_{rep}} \sum_{\nu_j \neq k\nu_{spin}} \frac{A_j}{\sin\left(\pi\nu_j/\nu_{spin}\right)} + \sum_{\nu_j = k\nu_{spin}} A_j\right] \qquad \textbf{(2-3)}$$

Although by means of equation **(2-3)** it is in principle possible to evaluate the effect of periodic signal with any frequency spectrum, there are three main periods in which we are interested for internal straylight evaluation, i.e.: the satellite spin period (~60 s), the sorption cooler compressor period (~667 s) and the sorption cooler complete period (~4000 s).

In the following table we report the estimated damping factors for the four LFI frequency channels relatively to 667 s and 4000 s. Of course for spin-synchronous effects the damping factor is 1 at all frequencies.

| 30 GHz | | 44 GHz | | 70 GHz | | 100 GHz | |
|---|---|---|---|---|---|---|---|
| 667 s | 4000 s | 667 s | 4000 s | 667 s | 4000 s | 667 s | 4000 s |

| | | | | | | | |
|---|---|---|---|---|---|---|---|
| 200 | 35 | 150 | 25 | 90 | 15 | 65 | 10 |

***Table 5-2*** *– Damping factors determined by measurement redundancy*

In addition to the reduction obtained by measurement redundancy we must also consider that an additional damping factor will come from post-processing the time-ordered data with destriping and/or map-making algorithms. These algorithms are able to recognise and remove spurious signal characterised by frequencies which are longer than the satellite spinning frequency.

In Figure 5-1 we show a curve representing the destriping damping factor of the peak-to-peak amplitude of sinusoidal periodic oscillations versus the period of the oscillation; this curve was obtained by applying the destriping algorithm of Burigana et al. [RD 10] (see also Maino et al. [RD 11] and references therein) and it is relative to a 30 GHz LFI detector. The graph shows that this additional factor increases approximately linearly with the period of the sinusoidal oscillation; the destriping algorithm, in fact, approximates the periodic effect on each scan circle with a constant level, and this approximation obviously works increasingly better with low-frequency oscillations. Combining the results given by equation (2-2) and by Figure 5-1 we have that for slow oscillations the total damping factor from the Time Ordered Data to the final map is roughly independent from the oscillation frequency.

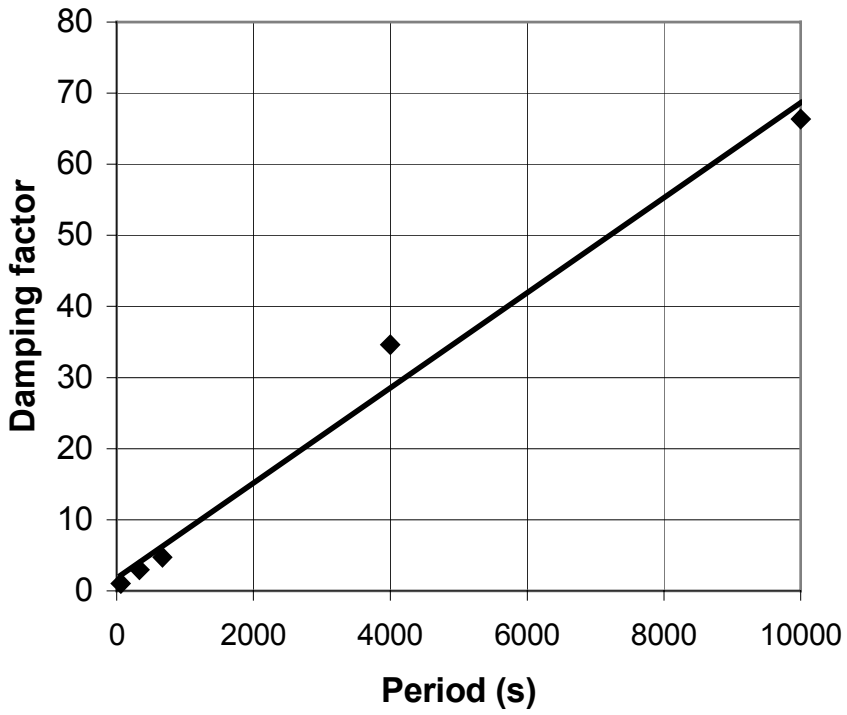


***Figure 5-1*** *– Destriping damping factor for periodic oscillations versus $\tau_f$ (the period of the fluctuation). Dots indicate the values obtained from maps while the solid line represents a linear interpolation.*

Of course the damping factor obtained by destriping is generally dependent both on the algorithm used and on other details like the position of the detector in the focal plane, the sampling frequency, the pixel size and the scanning strategy. The dependency, however, is rather weak, so that we can fix reference values (reported in the table below) for this additional damping at the main periods expected for internal straylight fluctuations (i.e. 60s, 667s, and 4000s).

| 60 s | 667 s | 4000 s |
|---|---|---|
| 1 | 5 | 30 |

***Table 5-3*** *– Damping factors determined by data post-processing (destriping)*

We now multiply the values in Table 5-2 by the values in Table 5-3 and obtain the total damping, $F_{tot}$, which is roughly independent from the fluctuation period (apart from spin-synchronous oscillations). In the following table we list the total damping factors for the four LFI frequency channels relatively to slow, non spin synchronous fluctuations (i.e. $\tau_f \geq 300\,\mathrm{s}$ ).

| 30 GHz | 44 GHz | 70 GHz | 100 GHz |
|---|---|---|---|
| 1000 | 750 | 450 | 330 |

***Table 5-4*** *– Total damping factors from instrument output to final map after destriping*

## 5.2 EXTERNAL STRAYLIGHT

Any celestial source could be a source of external straylight, due to the imperfect off–axis rejection of the entire optical system.
Actually, the Sun, the Moon, the Earth, the Planets, the HII regions, the diffuse Galactic emission, the CMB dipole are sources of straylight which contributes in different ways and levels to the different portions of the full detection beam pattern. This type of signal is inherently spin-synchronous.

In order to maintain the scientific capabilities of LFI, a requirement on the maximum straylight level has been set [AD 1]

> Straylight signal coming from clean sky will be below 1 μK. Here we define "clean" the portion of the sky outside a region of ± 10°(TBC) around the Galactic plane and outside a region of TBD deg around main celestial sources (Moon, Jupiter, Saturn).

### 5.2.1 Calculation of the External Straylight Induce Noise (ESIN)

The ESIN can be evaluated once the full radiation pattern and the source brightness distribution are known. With a given scanning strategy, the observations can be simulated and the added noise on the final map can be evaluated.

First of all, we distinguish between external straylight from celestial compact (or compact–like w.r.t. the main beam) sources and from celestial diffuse emission.
In general, at a given instant $t$ of the PLANCK observation, the contamination from a compact source with brightness temperature $T_{A,obj}$ is given by:

$$\delta T_{A,obj}(t) = \frac{\int_{4\pi} T_{A,obj}(\gamma,t)J(\gamma,t)d\Omega}{\int_{4\pi} J(\gamma,t)d\Omega} \approx \frac{T_{A,obj}(R/d)^2 \pi J(\gamma_{obj},t)}{\int_{4\pi} J(\gamma,t)d\Omega} \tag{5-4}$$

where $J(\gamma,t)$ is the antenna response along the direction identified by the unit vector $\gamma$; in the right hand expression, which is justified by the fact that $J$ can be considered constant over the small object solid angle, $\gamma_{obj}$ identifies the object direction, and $R$ and $r$ are object radius and distance from the spacecraft.

The straylight contamination from a diffuse component is derived from a convolution given, at a time $t$ , by

$$\begin{aligned}\delta T_{A,Comp}(t) &= \frac{\int_{4\pi} T_{A,Comp}(\gamma,t)J(\gamma,t)d\Omega}{\int_{4\pi} J(\gamma,t)d\Omega} = \\ &= \frac{\int_{MB} T_{A,Comp}(\gamma,t)J(\gamma,t)d\Omega}{\int_{4\pi} J(\gamma,t)d\Omega} + \frac{\int_{SL} T_{A,Comp}(\gamma,t)J(\gamma,t)d\Omega}{\int_{4\pi} J(\gamma,t)d\Omega} = \\ &= \delta T^{MB}_{A,Comp}(t) + \delta T^{SL}_{A,Comp}(t)\end{aligned} \tag{5-5}$$

where $J(\gamma,t)$ is the antenna response along the direction identified by the unit vector $\gamma$; and $T_{A,Comp}$ is the brightness temperature of the diffuse components. *MB* means the angular region of the main beam; *SL* is the angular region outside the main beam and then the angular region of the sidelobes.

Both equations (5-4) and (5-5) require that $J(\gamma,t)$ is well known. It is clear that the main problem of the ESIN calculation is the uncertainty on the knowledge of the radiation pattern itself. Modelisation requires extremely complex and time consuming calculations which are currently in progress. In the sidelobe region, the pattern is dominated by the diffraction on the edges of the surfaces of the satellite (the telescope at first, the baffle, the shields, the V – groves, the SVM, ...). Moreover, because of the complexity of the entire satellite, approximations on the geometry are mandatory (for instance, the edges can only be simulated as absolutely sharp structures, the multiple reflections and more than three consecutive scattering need to be neglected). Advanced and optimised codes are needed and, at the end, the electromagnetic model needs to be validated, in some way, by measurements.

### 5.2.2 External Straylight Requirements

In principle we can distinguish between two cases:

1. ESIN requirements which **can** be translated into requirements at instrument level. The galaxy straylight is mainly dependent on the feed design. In this case the required rejection level will be translated in edge taper requirements [4].
2. ESIN requirements which **cannot** be translated into requirements at instrument level. The Sun, Moon, and Earth rejection cannot be controlled by the edge taper. In this case only the rejection levels can be given [5].

[4] The galaxy straylight is dominated by the main spillover and marginally depends on the shield configuration.
[5] The rejection levels of Sun, Moon, and Earth signals depend mainly on the shielding structure design and scanning strategy (satellite), and marginally on the edge taper values (instrument).

Assuming that these two kind of requirements can be treated separately, the first one needs to be set according to the work devoted to the optimisation of the angular resolution and thus will be defined by means of optical simulations. Starting from Equation (5-4), the second one can be defined in the following way. Assuming a maximum level of contamination of 1 μK, the requirements of the rejection level of the pattern due to the compact sources is derived by:

$$\delta T_{A,obj}(t) = \frac{T_{A,obj}(R/d)^2 \pi J(\gamma_{obj},t)}{\int_{4\pi} J(\gamma,t)d\Omega} \leq 1\mu\text{K} \qquad (5\text{-}6)$$

By inverting the equation above we obtain the requirement on the pattern attenuation:

$$J(\gamma_{obj},t) \leq \frac{1\mu\text{K}}{T_{A,obj}} \cdot \frac{4\pi\sigma^2}{\pi} \cdot \left(\frac{d_{\min}}{R}\right)^2 \cong 6.1 \cdot 10^{-14} \cdot \frac{(FWHM[\text{arcmin}])^2}{T_{A,obj}[\text{K}]} \cdot \left(\frac{d_{\min}}{R}\right)^2 \qquad (5\text{-}7)$$

where $d_{min}$ is the minimum distance between the celestial source and the satellite, and σ is the beamwidth (the beam is assumed as gaussian). The calculations are reported in Table 5-5, for each frequency channel. The angular region at which the beam shall exhibit the rejection level is depending on the scanning strategy. Actually, could be of the order of 60°x60° for the Moon and less for the Sun and Earth. It is clear that major information can be derived by simulating the observation with a reasonable full pattern response, once the scanning strategy is defined (see [RD 7] and [RD 8] for simulations based on Carrier Configuration and COBRAS / SAMBA orbit).

| | | | 30 GHz | | 44 GHz | | 70 GHz | | 100 GHz | |
|---|---|---|---|---|---|---|---|---|---|---|
| FWHM | | | 36' | 30' | 29' | 24' | 17' | 14' | 12' | 10' |
| | | | req | goal | req | goal | req | goal | req | goal |
| Sun | Distance [Km] | $150 \times 10^6$ | 92 | 94 | 94 | 96 | 99 | 100 | 102 | 103 |
| | Radius [Km] | $7 \times 10^5$ | | | | | | | | |
| | Brightness [K] | 6000 | | | | | | | | |
| Earth | Distance [Km] | $1.5 \times 10^6$ | 78 | 80 | 80 | 82 | 85 | 87 | 88 | 89 |
| | Radius [Km] | $6.4 \times 10^3$ | | | | | | | | |
| | Brightness [K] | 300 | | | | | | | | |
| Moon | Distance [Km] | $1.1 \times 10^6$ | 69 | 71 | 71 | 73 | 76 | 77 | 79 | 80 |
| | Radius [Km] | $1.75 \times 10^3$ | | | | | | | | |
| | Brightness [K] | 250 | | | | | | | | |
| Jupiter | Distance [Km] | $627 \times 10^6$ | 45 | 46 | 47 | 48 | 51 | 53 | 54 | 56 |
| | Radius [Km] | $71 \times 10^3$ | | | | | | | | |
| | Brightness [K] | 180 | | | | | | | | |
| Saturn | Distance [Km] | $1276 \times 10^6$ | 36 | 38 | 38 | 40 | 43 | 44 | 46 | 47 |
| | Radius [Km] | $60 \times 10^3$ | | | | | | | | |
| | Brightness [K] | 150 | | | | | | | | |

***Table 5-5*** *– System level reference requirements. The table reports the rejection level, below the main beam peak, for Sun, Earth, Moon, Jupiter and Saturn.*

Differently from Sun, Earth and Moon, Jupiter and other external planets (as well as point sources) can contaminate the map through the "intermediate" sidelobes, i.e., the sidelobes immediately adjacent to the main beam: this is where the highest contamination comes from. Jupiter is the strongest compact source that can actually pass into the beam, and data must be corrected or excluded when it falls within the contour at values reported in Table 5-5.

Some Galactic sources, such as HII regions, can be strong sources in the LFI beams and their effects in the sidelobes must be checked. However, these sources are present mainly in the Galactic plane, and are likely to affect only the main and intermediate beam, when the observed sky will be dominated by the Galactic emission.

> The straylight effect from small-solid-angle sources in the far sidelobes can be extremely nasty for the Planck mission. In fact, their contribution to the signal, as the spacecraft spins, will be modulated by the detailed features of the far side lobes. Since it will be impossible to map the far sidelobes with high accuracy and high resolution, there will be no credible way to remove the effect of such sources from the data."
>
> It should be noted that the numbers reported in Table 5-5 do not include any margin on the uncertainty on the pattern knowledge (in flight). Therefore, depending on the uncertainty, these requirements have to be carefully confirmed or revised.

#### 5.2.2.1.1 Galactic emission straylight

Sidelobe structure sweeping across the Galaxy can produce artefacts in any direction. We have simulated this effect, convolving the LFI radiation pattern with a model of Galactic emission (see [RD 5] for more details). At LFI frequencies, Galaxy straylight is crucial at the lowest frequencies, due to the increasing synchrotron emission with wavelength. We distinguish 3 pattern regions at different angular distance $\theta$ from the beam centre:

a) *Main beam*: the beam portion from beam centre to $\theta < 1.2°$
b) *Intermediate beam*: the region $1.2° < \theta < 5°$, which contains about 0.6% of the integrated power
c) *Far beam*: the region $\theta > 5°$, which contains about the 1% of the integrated power. The main spillover accounts for $\approx 0.1 \div 0.2$ % of the integrated power.

The Galaxy model assumed for the ESIN calculation is described extensively in [RD 3] and [RD 5]. We refer to these papers for details.

We compute separately the convoluted signals from these three pattern portions (assuming the *carrier* beam patterns). The simulated data streams for a 1 year mission (in ecliptic coordinates) are reported in Figure 5-2.

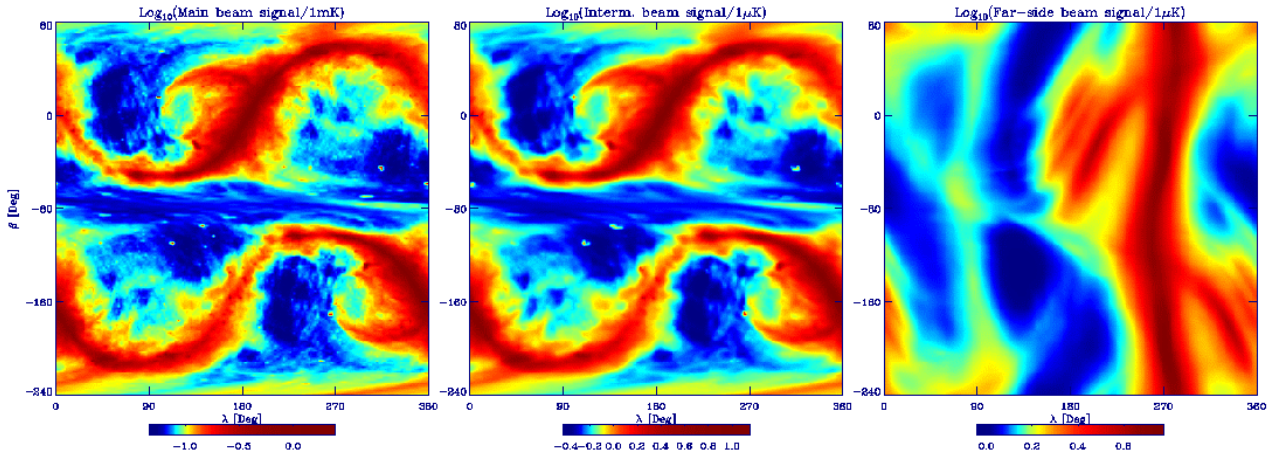


***Figure 5-2***– *Simulated data stream from all scan circles ($\alpha$ = 80°) for main beam (left panel), intermediate beam (centre), far beam (right). Note the different colour scales. The ecliptic coordinates $\lambda$ and $\beta$ refer to the direction of the telescope.*

As one expects, straylight from the intermediate beam roughly follows the structure observed by the main beam.

The ESIN from far pattern exhibits four main features, two introduced by the main spillover (see Figure 5-2) and two by the pattern close to the main beam, as they cross the Galactic plane. The azimuthal asymmetry of the main spillover reflects in the large difference between the two halves (along x axis) of the right panel. This difference can be used to remove to first order the effect. The effect from the intermediate beam peaks at about 10 μK, a value comparable with the sensitivity per pixel. However this happens in regions close to the Galactic plane, where the signal from the Galaxy in the main beam prevents accurate CMB measurements. This straylight effect is not crucial for the determination of Galactic emission, which is about 3 order of magnitude larger. The contamination from the far pattern peaks at about 4 μK. This effect is smaller than that from intermediate pattern, but it extends to high Galactic latitudes, where the LFI sensitivity is higher and we expect to extract maximum information on CMB fluctuations and polarisation.

| | 30 GHz | 100 GHz |
|---|---|---|
| Rejection level for Galaxy | 65 | 75 |

***Figura 1 –*** *Top level Requirements for Galaxy Contamination. Pattern Rejection levels at 30 and 100 GHz. Numbers are in dB below the main beam peak.*

## 5.3 INTERNAL STRAYLIGHT

Thermal emission from all components of the spacecraft produces a signal which is not easily distinguishable from signals due to sources in the main beam. The time variation of the straylight signal from these sources is due to fluctuations in the temperature of emissive components.

We can identify three main sub-units in the satellite that can give a contribution to the internal straylight, i.e.: (i) the telescope, (ii) the baffle, (iii) the 50K V-Groove. In general we divide the different straylight contributions into three different categories, i.e.: (i) random thermal fluctuations of emissive surfaces, that will have the main effect of increasing the radiometer noise, (ii) periodic spin-synchronous thermal

fluctuations, that will generate signal oscillations that will not be damped by the measurement strategy, and (iii) periodic non spin synchronous thermal fluctuations, that will generate signal oscillations that will be reduced in amplitude by the measurement strategy and by destriping/map-making algorithms.

In Table 5-6 we report the total error budget on the final measured maps.

| Source | Error from random fluctuations (% of 1-sec sensitivity) | Error from spin synch. signals (μK) | Error from other periodic signals (μK) |
|---|---|---|---|
| Telescope | 2% | 0.5 | 0.55 |
| Baffle | 2% | 0.5 | 0.55 |
| Cold V-groove | 2% | 0.5 | 0.55 |
| Total | 3.5% | 0.87 | 0.95 |

***Table 5-6*** *– Breakdown of LFI internal straylight*

Note that the requirements relative to random temperature fluctuations of emissive surfaces are given in terms of the 1-second radiometer sensitivity, $\delta T_{1\text{-sec}}$. Goal and requirement values for $\delta T_{1\text{sec}}$ in antenna temperature (see [AD 1]) are reported in the following table.

| | 30GHz | | 44GHz | | 70GHz | | 100GHz | |
|---|---|---|---|---|---|---|---|---|
| | Goal | Req | Goal | Req | Goal | Req | Goal | Req |
| $\delta T_{1\text{sec}}$ (μK × √s) | 175 | 234 | 209 | 278 | 274 | 365 | 342 | 460 |

***Table 5-7*** *– Goals and requirements for $\delta T_{1\text{sec}}$ according to the LFI systematic error budget*

No that with the term "periodic signals" we specifically refer to fluctuations that are characterised by a period which is much longer than the spin period, i.e. > 300 s. This approximation can be considered generally applicable to the PLANCK environment, where the main source of periodic oscillations in the satellite is the Sorption Cooler, characterised by the two main periods of ~667 s (single compressor cycle) and of ~4000 s (cooler cycle).

### 5.3.1 Calculation if the Internal Straylight Induced noise (ISIN)

To establish requirements on the maximum allowable thermal fluctuations of PLANCK emissive surfaces we start considering a fluctuation $\delta T_{\text{Phys, surf}}$ of the temperature of a given surface. This fluctuation will couple with LFI feed-horns such that the antenna temperature fluctuation at the feed aperture is given by:

$$\delta T_{\text{A, surf}} = j(\nu)\varepsilon(\nu)\delta T_{\text{Phys, surf}} \tag{5-8}$$

where $\varepsilon(\nu)$ is the surface emissivity and $j(\nu)$ is the optical coupling of the feed with the emissive surface. Both are assumed constant on the time scales of interest here.

The function $j(\nu)$ can be written as:

$$j(\nu) = \int J_{NF}(\nu, x, y, z) D_{Surf}(x, y, z) \mathrm{dxdydz} \quad (5\text{-}9)$$

where $J_{NF}$ is the normalised near field feed response and $D_{surf}$ defines the solid angle subtended by the emissive surface.

### 5.3.2 Internal Straylight Requirements

In this section we start from the scientific requirements on internal straylight given in Table 5-6 to derive requirements on the thermal stability of the relevant emissive surfaces. In this process we need to know the transfer function from the radiometer output to the map (which is provided by the damping factors in Table 5-4) and to estimate emissivities, beam patterns and solid angles that enter in equations **(5-8)** and **(5-9)**.

In the next subsections we perform some simple calculations to estimate such requirements. Note that these calculations use conservative and highly simplifying assumptions concerning the optical coupling between the feed-horns in the focal plane and the radiating surfaces. Therefore the requirement values should be understood as order-of-magnitude values that will be refined **only in the case they introduce a criticality in the development of the spacecraft.** It must be underlined, however, that even though more refined simulations can give a more precise estimate of these values, **it is unlikely that the estimated order of magnitude will change**, so that the values reported here should be regarded as realistic requirements as far as the order of magnitude is concerned.

#### 5.3.2.1 Telescope

Currently it is specified (see [AD 2]) that the PLANCK telescope will have a reflectivity between 0.995 (beginning of life) and 0.975 (end of life, with a goal of 0.99), from 25 GHz to 1000 GHz[6]. Therefore, assuming that thermal fluctuations of the secondary mirror will be the most important source of systematic errors we can consider an average telescope emissivity of about 0.015, and a coupling to the feed $j \approx 1$.

We can now establish preliminary requirements based on the budget specified in Table 5-6. Note that the requirements below apply to the *average* temperature of the telescope, not to thermal fluctuations of small portions of it.

##### 5.3.2.1.1 Random thermal fluctuations

If we consider random thermal fluctuations, it is possible to estimate the fluctuation level that produces a variation in $\delta T_{1sec}$ equal to the maximum allowed value, $\delta T_{random} = \frac{\delta T_{1sec}^{max}}{\varepsilon\, j}$, where $\delta T_{1sec}^{max}$ is calculated using values in Table 5-6 and Table 5-7. Values of $\delta T_{random}^{req}$ for the four LFI frequencies are reported in Table 5-8

| | 30 GHz | 44 GHz | 70 GHz | 100 GHz |
|---|---|---|---|---|
| $\delta T_{random}$ ($\mu K \times \sqrt{s}$) | 310 | 370 | 490 | 610 |

***Table 5-8*** *– Values of $\delta T_{random}$ for telescope random thermal fluctuations*

[6] It is supposed that only the temperature fluctuations of the secondary reflector is contributing to the internal straylight. The emissivity values are referred to a single reflector.

Considering that the 30 GHz channel is the most sensitive to telescope random thermal fluctuations we require that the random thermal fluctuations of the telescope will be at a level less than 300 mK × √s.

#### 5.3.2.1.2 Spin-synchronous fluctuations

Proceeding in an analogous way, we can estimate the fluctuation level that produces a spin-synchronous signal equal to the allowed telescope budget of 0.5 μK per pixel (see Table 5-6). Considering that for spin synchronous fluctuations the damping factor from Time Ordered Data to the final map equals 1, we can formulate to the following requirement: Spin synchronous thermal fluctuations of PLANCK telescope will be less than 33 μK (TBC).

#### 5.3.2.1.3 Other periodic (slow) fluctuations

Starting from the budget in Table 5-6 and considering the damping factor values reported in Table 5-4 we can estimate the fluctuation level that generates a variation in the observed signal equal the allowed budget of 0.55 μK: $\delta T_{\text{periodic}}^{\max} = \frac{F_{\text{tot}}}{\varepsilon\, j} 0.55\,\mu\text{K}$. Note that the damping factor $F_{\text{tot}}$ is different for the four frequency channels, so that we get four different values for $\delta T_{667s}^{\max}$, ranging from 36 mK (@ 30 GHz) to 12 mK (@ 100 GHz). In order to be compliant with the budget in Table 5-6 we define the following requirement: Periodic thermal fluctuations of PLANCK telescope will be less than 10 mK (TBC). This requirement applies only to the harmonics which are NOT spin-synchronous. Note the above requirement do not apply for spin-synchronous harmonics, which need to be compliant with the global requirement for spin-synchronous fluctuations.

### 5.3.2.2 Baffle

Thermal fluctuations of the baffle represent another potential source of systematic errors. To evaluate the impact of such effects it is possible, in principle, to use equations **(5-8)** and **(5-9)** in a similar way to that used in the previous section. Although accurate calculations involve optical simulations to calculate the coupling factor $j(\nu)$, it is possible to make an order-of-magnitude estimate for a simpler configuration of an on-axis feed with the beam patters sketched in Figure 5-3. In practice we assume zero response in the central region (corresponding to the secondary mirror) and in the region behind the feed-horn. In the remaining part we assume a constant response of –30dB corresponding to the current edge taper requirements. Note that this is a conservative approach, since at large angles the sidelobe level will be significantly lower than the edge taper value.

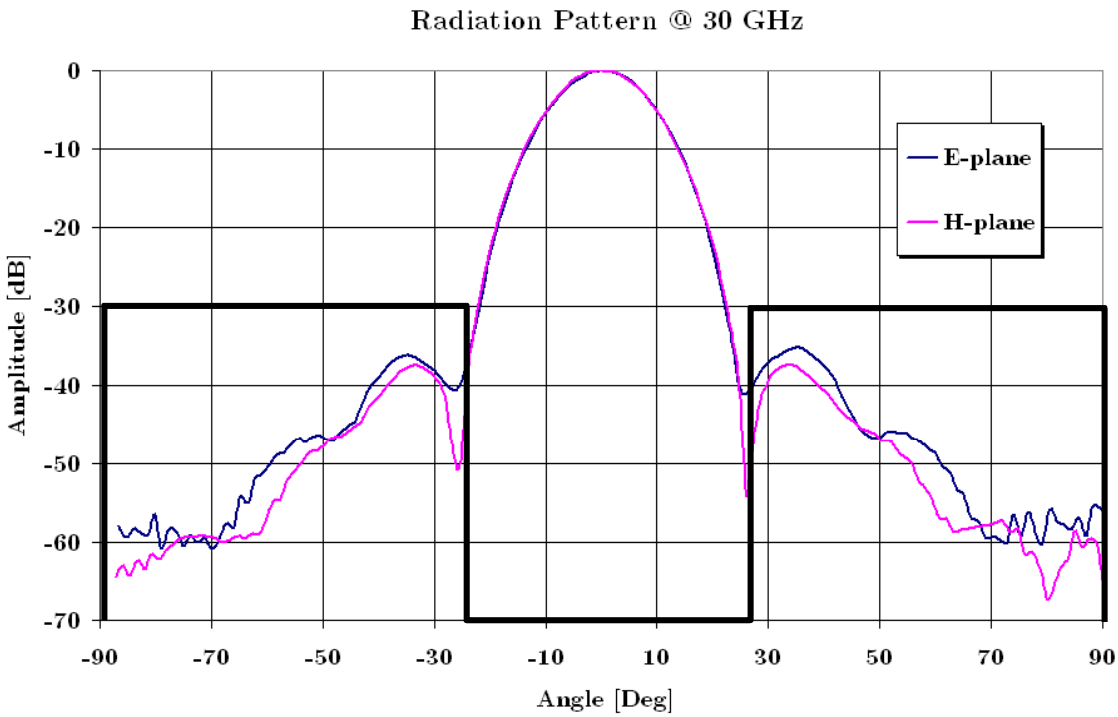


***Figure 5-3*** *– Simplified beam pattern (black solid line) for the calculation of the SIN induced by thermal fluctuations of the baffle. The complete beam pattern represents the measured pattern of the 30 GHz EBB feed-horn*

The solid angle relative to this region is $D_{surf} = \pi(2 - \sin(\theta_{tel})^2)$ , where $\theta_{tel}$ represents the semi aperture of the secondary mirror (~ 22°).

Another quantity that needs to be specified is the emissivity of the inner part of the baffle. Currently there are no specifications defined for this emissivity, and the only available information is that *"the internal face of the baffle is Aluminum coated, as for the primary and secondary reflectors"*, as written in [RD 6]. If we now consider that the baffle surface will be rougher that the telescope, we can reasonably expect a higher emissivity. Considering our current lack of information we will assume an emissivity one order of magnitude higher than the telescope, i.e. $\varepsilon_{baffle} = 0.15$.

Proceeding in a similar way as in section 5.3.2.1 we can define requirements for thermal stability of the baffle source by using equations **(5-8)** and **(5-9)** with the simplifying assumptions discussed above. These requirements are summarised in the table below.

| | |
|---|---|
| $\delta T_{random}$ (mK × √s) | 5.34 |
| $\delta T_{SS}$ (mK) | 0.57 |
| $\delta T_{periodic}$ (K) | 0.2 |

***Table 5-9*** *– Thermal stability requirements for the baffle surface*

### 5.3.2.3 3rd V-groove

Thermal fluctuations of the 50K V-groove represent the third most important potential source of Internal Straylight. Here we proceed similarly to the previous sections by estimating the optical coupling factor in a simplified geometrical environment, sketched in Figure 5-4. In practice we assume that thermal fluctuations in the 50K V-Groove will couple with the feed horns in the focal plane in a solid angle of 45° total aperture.

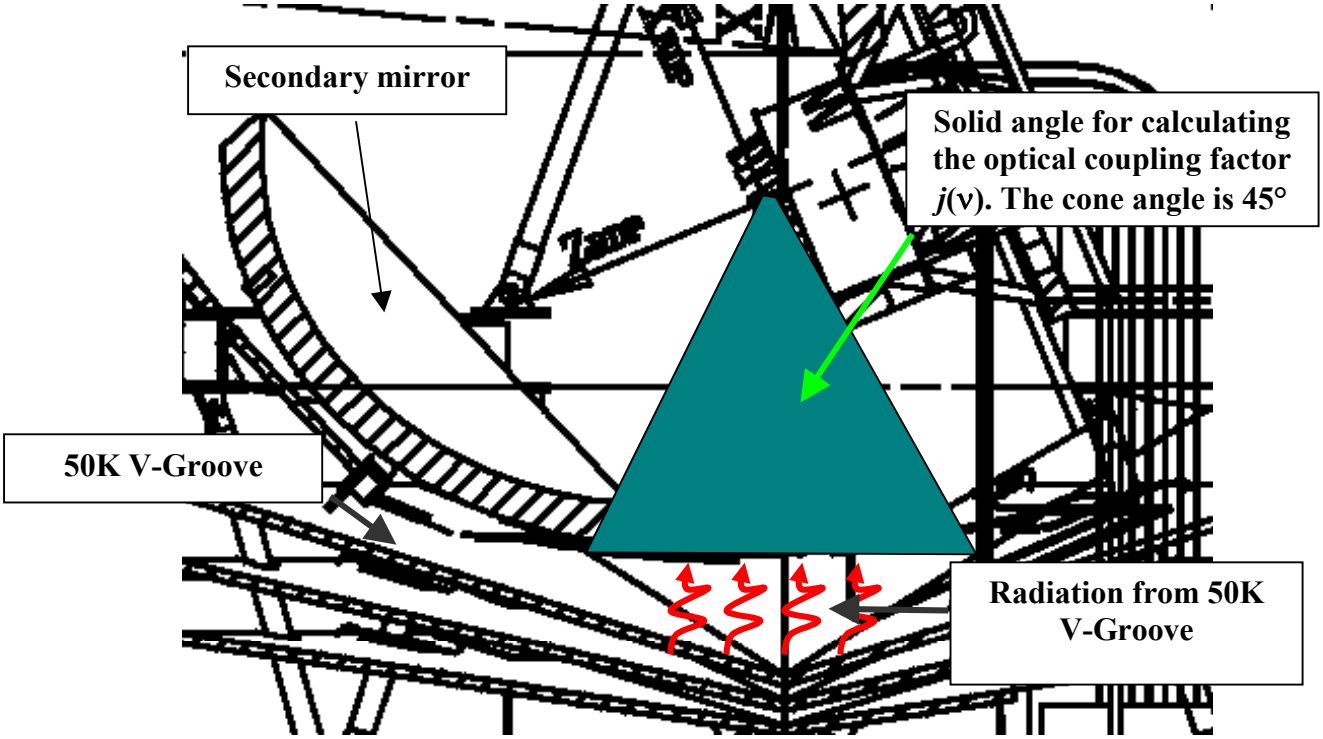


***Figure 5-4*** *– Simplified geometry for the evaluation of the Straylight Induced Noise caused by thermal fluctuations of the cold V-Groove. We assume that the feed horns are sensitive to such fluctuations in a solid angle of 45° total aperture as depicted in the figure*

Therefore in this case we can assume a solid angle of equal to $D_{surf} = \pi \sin(\theta)^2$ (where $\theta \sim 22.5°$ is the cone half angle). As for the beam pattern in this region we have conservatively assumed a value of –30 dB, which corresponds to the current edge taper requirements.

The surface emissivity of the 50K V-Groove in the region indicated in Figure 5-4 is required to be low, of the order of 0.02 (see [AD 3] page 5-42). The thermal stability requirements obtained by our calculations performed with the above assumptions are summarised in the table below.

| | |
|---|---|
| $\delta T_{random}$ (mK × √s) | 508 |
| $\delta T_{SS}$ (mK) | 54.5 |
| $\delta T_{periodic}$ (K) | 19.5 |

***Table 5-10** – Thermal stability requirements for the 50K V-groove surface*

### 5.3.3 Conclusions

In this section we have derived requirements on the thermal stability of various internal optical interfaces starting from the high level scientific requirements on internal straylight which are summarised in Table 5-1. From our analysis we conclude that the most stringent thermal stability is required on the telescope, while other interfaces (like the baffle and the cold V-groove) are expected to have a much lesser impact from the internal straylight point of view. Future thermal simulation work will provide a confirmation of the consistency of these requirements with the expected thermal stability of such interfaces.